



4-25-2016

# The Role of Continuum States in the Field Ionization of Rydberg Atoms

Michael P. Vennettilli

Ursinus College, [mivennettilli@ursinus.edu](mailto:mivennettilli@ursinus.edu)

Adviser: Thomas Carroll

Follow this and additional works at: [https://digitalcommons.ursinus.edu/physics\\_astro\\_hon](https://digitalcommons.ursinus.edu/physics_astro_hon)



Part of the [Atomic, Molecular and Optical Physics Commons](#)

**Click here to let us know how access to this document benefits you.**

## Recommended Citation

Vennettilli, Michael P., "The Role of Continuum States in the Field Ionization of Rydberg Atoms" (2016). *Physics and Astronomy Honors Papers*. 2.

[https://digitalcommons.ursinus.edu/physics\\_astro\\_hon/2](https://digitalcommons.ursinus.edu/physics_astro_hon/2)

This Paper is brought to you for free and open access by the Student Research at Digital Commons @ Ursinus College. It has been accepted for inclusion in Physics and Astronomy Honors Papers by an authorized administrator of Digital Commons @ Ursinus College. For more information, please contact [aprock@ursinus.edu](mailto:aprock@ursinus.edu).

THE ROLE OF CONTINUUM STATES IN THE FIELD  
IONIZATION OF RYDBERG ATOMS

by

Michael Vennettilli

Department of Physics  
Ursinus College

April 25, 2016

Submitted to the Faculty of Ursinus College in fulfillment of  
the requirements for Honors in the Department of Physics.



Copyright © April 25, 2016 by Michael Vennettilli  
All rights reserved



# Abstract

In an experiment performed by our collaborators at Bryn Mawr, we excite rubidium-85 to a coherent superposition of the different  $|m_j|$  splittings of the  $37d_{5/2}$  state induced by a small electric field. After waiting for some variable delay time, apply a time-dependent electric field to ionize the atom and record the ionized current that arrives at the detector. Due to the initial superposition, we observe an interference pattern that depends on the delay time. This thesis describes my continued work with Dr. Carroll to develop a computational model of this experiment. Our initial method of determining the current involved a semi-classical approach that did not accurately describe the phase, so the more recent developments in more work have focused on including the continuum states in our calculation.



## Acknowledgments

I would like to begin by thanking Dr. Thomas Carroll. He played a large part in my decision to study physics, and I have benefited immensely from his mentorship in physics, research, and beyond. He has always been accessible, helpful, and patient whenever I have encountered difficulties, confusion, or stumbling blocks.

I would like to thank our collaborators at Bryn Mawr, namely, Dr. Michael Noel and Rachel Feynman. They were responsible for carrying out the experimental work in our project. Without their contributions, this project would not have been possible.

I would like to thank my fellow students Jake Hollingsworth, Tamas Budner, and Ryan Zmiewsky, who I shared an awesome research experience with during our Summer Fellows project. I would also like to express extended gratitude towards Jake. We spent a lot of time both before and after Summer Fellows working on research together; our discussions have always been enlightening.



# Contents

<b>List of Figures</b>	<b>ix</b>
<b>1 Introduction</b>	<b>1</b>
1.1 Introduction . . . . .	1
1.2 Experiment . . . . .	2
<b>2 Avoided Crossings and Non-adiabatic Transitions</b>	<b>5</b>
2.1 A Toy Model . . . . .	5
2.2 Non-Adiabatic Transitions . . . . .	8
<b>3 Traversing the Stark Map</b>	<b>11</b>
3.1 The Stark Effect . . . . .	11
3.2 Stark Maps and Time Evolution . . . . .	16
3.3 The Semi-classical Ionization Current . . . . .	20
<b>4 Including the Continuum States</b>	<b>25</b>
4.1 Hypergeometric Functions . . . . .	26
4.1.1 The Confluent Hypergeometric Equation . . . . .	28
4.2 Hydrogenic Continuum States . . . . .	29
4.3 Coupling to the Continuum . . . . .	32
<b>5 Future Work</b>	<b>35</b>



# List of Figures

1.1	Timing diagram for the ionization experiment. The delay time is a variable. . . . .	2
2.1	Spectrum of the perturbed Hamiltonian as a function of one of the perturbing parameters. The red lines correspond to the case where both of the other parameters are zero, while at least one of the other parameters is non-zero for the black lines. . . . .	7
3.1	Stark map for the $ m_j  = 1/2$ states of $^{85}\text{Rb}$ . The $n = 43, 44$ manifolds are shown with the $s, p, d$ states of larger $n$ that lie between them. Note that the energies depend on the electric field and that each state participates in a large number of avoided crossings. . . .	17
3.2	Portion of the Stark map where the initial state was a superposition of the different $ m_j $ components of the $37d_{5/2}$ state. Red, blue, and green correspond to $ m_j  = 1/2, 3/2,$ and $5/2$ respectively. The intensity of the color scales with the probability of finding the electron in that state. The black curve is the classical ionization threshold. .	20
3.3	Experimental (a) and theoretical (b) ionization currents as functions of time. The colors here are unrelated to those in Fig. 3.2. . . . .	23
3.4	(a,b) Area under the regions in Fig. 3.3 (a,b) (respectively) as a function of the delay time. The color of the curves corresponds to the region that is integrated. In (a), the red and blue are completely out of phase, while this is not the case in (b). . . . .	23
4.1	Potentials for an attractive Coulomb interaction and a uniform electric field with $x = y = 0$ . Since the sum of the potentials is unbounded below as one goes to infinity, there are no permanently bound states. . . . .	26



# Chapter 1

## Introduction

### 1.1 Introduction

A Rydberg atom is an atom whose outermost electron has been excited to a state with a large principal quantum number  $n$ . These atoms strike a balance between the simplicity of their description and providing opportunities for interesting physics. When one is only interested in the outermost electron, a Rydberg atom can be thought of as an exaggerated hydrogen atom, as the Rydberg electron is localized far away from the positive core that is comprised of the nucleus and inner electrons. These atoms are a strong candidate for use in quantum control or low temperature experiments, since they have a large dipole moment that makes them very sensitive to applied fields.

Selective-field ionization is a routinely used experimental technique that uses a time-dependent electric field to selectively ionize particular states. However, the quantum dynamics of an electron in a time-dependent electric field are rich and interesting in their own right. As the electric field is varied, the electron goes through many avoided crossings and will quickly become a complex superposition. Stoneman et al. [1] have used techniques from photo-ionization to probe this behavior. This behavior is a particular instance of the more general phenomenon of non-adiabatic

transitions. One can perform interferometry with these avoided crossings, and this has been used to observe a geometric phase in superconducting qubits [2]. This has also been used to detect error in qubits that arise from interactions with the environment that spoil the coherence of the qubit [3].

## 1.2 Experiment

This work is focused on the computational modeling of an experiment performed by our collaborators at Bryn Mawr [4]. Our purpose was to probe the behavior of Rydberg atoms in response to a time-dependent electric field. In particular, we did so by exciting a Rydberg atom in a coherent superposition of nearly degenerate states, used an electric field to ionize the Rydberg state, and then analyzed the resulting ionization current. The timing diagram that shows the steps and their timescales is shown in Fig. 1.1. In our experiment, we chose to work with rubidium-85. We started by cooling the rubidium gas in a magneto-optical trap (MOT) to  $200 \mu\text{K}$ .

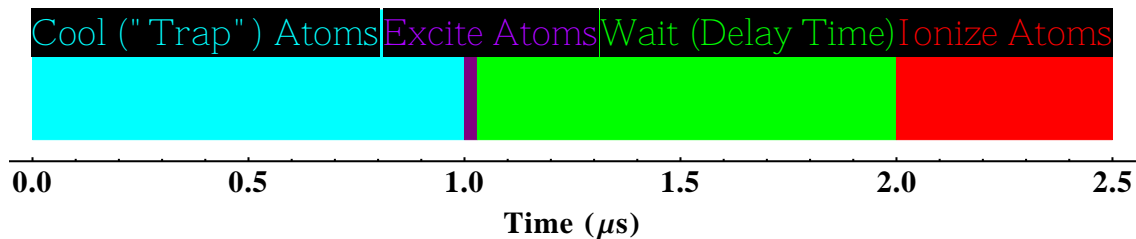


**Figure 1.1:** Timing diagram for the ionization experiment. The delay time is a variable.

We chose to work with the  $37d_{5/2}$  state, that is,  $n = 37$ ,  $l = 3$ , and  $j = 5/2$ . A static electric field was applied to break the degeneracy of the  $m_j = 1/2, 3/2$ , and  $5/2$  energy levels. The excitation scheme is achieved in three steps. The

$5s_{1/2} \rightarrow 5p_{3/2}$  transition is driven by the MOT's trapping lasers, which have a wavelength of 780 nm. The next step is the  $5p_{3/2} \rightarrow 5d_{5/2}$  transition. This is achieved by pulsing a 776 nm for 10  $\mu$ s at a rate of 20 pulses/seconds. After this step, some of the atoms will decay via  $5d_{5/2} \rightarrow 6p_{3/2}$ . After the end of the 776 nm pulse, we apply a 1019 nm laser in a short pulse to induce the  $6p_{3/2} \rightarrow 37d_{5/2}$  transition. Since the pulse is localized in time, it has some width. This width is large enough so that the final excitation is a coherent superposition of all three  $|m_j|$  states. The volume occupied by the excited atoms is the region where the 776 nm and 1019 nm lasers overlap, and this was chosen to coincide with the zero of the MOT's magnetic field.

After preparing the Rydberg atoms, we wait for some variable delay time and then apply our ionization pulse. Since the degeneracy of the  $|m_j|$  components is broken, the delay time allows the components of the superposition to accrue relative phases. The ionizing field pulse is nearly linear in time. As the field increases, the amplitude will disperse through many states due to the couplings between different energy levels; the state will be a complicated superposition near the classical ionization threshold. Since the ionization threshold is energy dependent, different states will ionize at different times, so we expect our ionization current to be extended in time. However, if parts of the different  $|m_j|$  components ionize at the same time, their relative phases will create an interference pattern as a function of the delay time.



# Chapter 2

## Avoided Crossings and Non-adiabatic Transitions

### 2.1 A Toy Model

In the Stark effect, a uniform electric field is applied to an atom. The presence of this field couples different eigenstates together by producing off-diagonal terms in the Hamiltonian. As the electric field is varied, the energies of the states will vary, as per standard perturbation theory [5]. If two states are coupled by this perturbation, those energy levels will never cross, that is, they will never have the same energy at a given electric field. Furthermore, if we produce a Stark map that shows the bound energies as a function of the electric field, we will see that the energies of coupled states that approach each other will deflect away from each other before intersecting; this is called an avoided crossing. In this section, we will cover a simple, two-state model to illustrate the effect of adding a perturbation to a Hamiltonian and show that off-diagonal couplings lead to avoided crossings.

We will consider a simplified model that illustrates these phenomena. Suppose

that we have some initial, unperturbed Hamiltonian  $H_0$  given by

$$H_0 = \epsilon \sigma_z = \begin{bmatrix} \epsilon & 0 \\ 0 & -\epsilon \end{bmatrix}, \quad (2.1)$$

where  $\epsilon$  is a real number. The energies of the unperturbed system are clearly  $\pm\epsilon$ . We can generally ignore multiples of the identity matrix; these merely shift the energy levels by a constant since they commute with everything.

Now we will consider adding a perturbation  $H_p$  to create a new Hamiltonian  $H = H_0 + H_p$ . Ignoring multiples of the identity, the most general Hermitian perturbation has the form

$$H_p = \alpha \sigma_x + \beta \sigma_y + \Delta \epsilon \sigma_z = \begin{bmatrix} \Delta \epsilon & \alpha - i\beta \\ \alpha + i\beta & -\Delta \epsilon \end{bmatrix},$$

for real numbers  $\alpha$ ,  $\beta$ , and  $\Delta \epsilon$ . For convenience, we will define  $\epsilon' = \epsilon + \Delta \epsilon$ , so our perturbed Hamiltonian is

$$H = \alpha \sigma_x + \beta \sigma_y + \epsilon' \sigma_z = \begin{bmatrix} \epsilon' & \alpha - i\beta \\ \alpha + i\beta & -\epsilon' \end{bmatrix}. \quad (2.2)$$

It is a straightforward exercise in linear algebra [6, 7] to show that the eigenvalues of this matrix are

$$E_{\pm} = \pm \sqrt{(\epsilon')^2 + \alpha^2 + \beta^2}.$$

If any two of the parameters  $\epsilon'$ ,  $\alpha$ , or  $\beta$  are zero, and we plot the spectrum as a function of the third parameter, we will find a crossing. In this case, it turns out that the Hamiltonian can be cast into the form of our unperturbed Hamiltonian in Eq.

2.1 without coupling. Our unperturbed Hamiltonian had no off-diagonal couplings, which are necessary to observe avoided crossings. In light of these considerations, we will take one of them to be non-zero. If we choose to plot the spectrum as a function of  $\beta$ , then the sum  $(\epsilon')^2 + \alpha^2$  is strictly positive. I have plotted the spectrum of our perturbed Hamiltonian in Fig. 2.1. The vertical axis indicates the energy, while the horizontal axis indicates the value of  $\beta$ . The red lines show the spectrum for  $(\epsilon')^2 + \alpha^2 = 0$ , while the black lines show the spectrum for  $(\epsilon')^2 + \alpha^2 > 0$ . As I argued earlier, we do see that the red lines cross, while the black lines deflect away from each other, as we would expect at an avoided crossing.

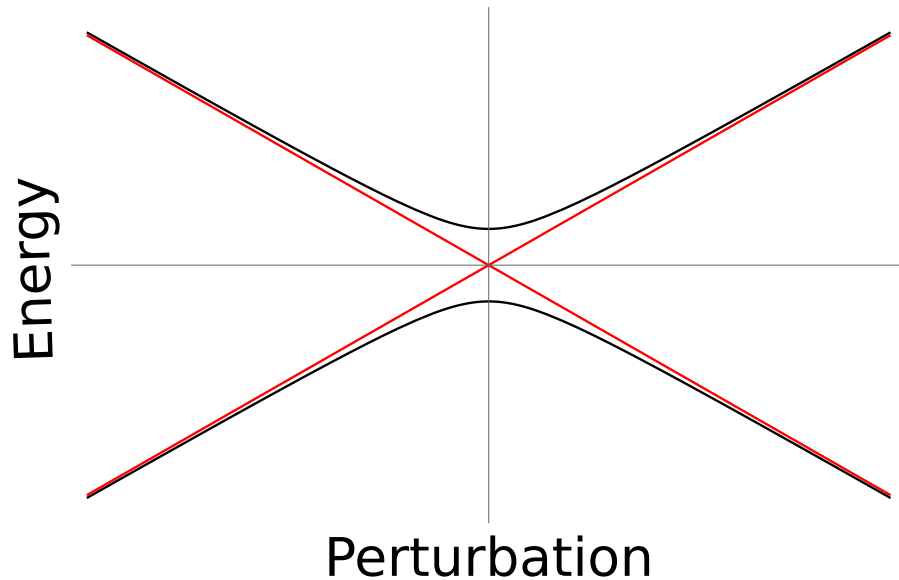


**Figure 2.1:** Spectrum of the perturbed Hamiltonian as a function of one of the perturbing parameters. The red lines correspond to the case where both of the other parameters are zero, while at least one of the other parameters is non-zero for the black lines.

## 2.2 Non-Adiabatic Transitions

In our work, we will concern ourselves with the dynamics of an electron that moves through a large number of avoided crossings due to a time-dependent perturbation; the purpose of this section is to give an understanding of this behavior. This will be achieved by considering some extreme, but analytically tractable, cases and moving on to discuss a more accurate treatment. In the case that the perturbation is changed arbitrarily slow, one may intuitively believe that the electron stays in the same state. This intuition can be proven, and this is the content of the adiabatic theorem [8]. To put things precisely, suppose that we have a time-dependent Hamiltonian  $H(t)$  whose eigenstates are labeled by some quantum number  $n$ :

$$H(t) |\psi_n(t)\rangle = E_n(t) |\psi_n(t)\rangle.$$

A general state is a superposition of these states, and we will denote the coefficients for each of the states by  $c_n(t)$ . If the time-dependent term in  $H(t)$  is turned on at  $t = 0$ , then the adiabatic theorem states that

$$|c_n(t)|^2 = |c_n(0)|^2,$$

for all time  $t$  and each  $n$ . Although there are a host of interesting phenomena in the adiabatic limit, such as geometric phases, and it is nice that we can rigorously justify our intuition, the dynamics of the amplitude in this limit are entirely uninteresting; nothing changes!

The other extreme example occurs when the Hamiltonian changes very quickly. In this case, the dynamics are more subtle. For simplicity, consider a two-state

system. If the two states do not couple, that is, there are no non-zero off-diagonal matrix elements for all times  $t$ , then the probability of finding the particle in either state is constant. The situation where the two states do couple together is more involved. This case was worked out by Rubbmark et al.; I will not reproduce the calculation here, but the curious reader is encouraged to read their paper [9]. In their model, the energies of the system are linear when the off-diagonal matrix elements are neglected and the perturbation is varied linearly as a function of time. If the system was in one state at  $t = -\infty$ , then the probability of finding it in the other state at  $t = +\infty$  is given by the Landau-Zener formula

$$P = \exp \left( -2\pi \frac{|\langle 1|V|2 \rangle|^2}{|d\omega/dt|} \right), \quad (2.3)$$

where  $\langle 1|V|2 \rangle$  is the off-diagonal matrix element and  $d\omega/dt$  is difference in the rates of change for the energies when the off-diagonal elements are neglected. It is helpful to study some limiting cases of this formula. In the case where the perturbation is changed slowly,  $d\omega/dt$  tends to 0 and the transition probability tends to 0 as well. This result seems reasonable, as the conditions are precisely those that satisfy the adiabatic theorem. We find a more surprising consequence in the other limit. As  $|d\omega/dt|$  becomes arbitrarily large, we find that the transition probability approaches 1 and the particle will be always be found in the other state! Although the only formula only describes asymptotic behavior, one can regard the amplitude as being transferred between the states at the avoided crossing, as transitions do not occur in the absence of couplings. Indeed, more direct calculations show that most of the amplitude is transferred near the avoided crossing.

Of course, experimentally accessible situations fall somewhere between these two extremes. We can't change a quantity by an infinitely large amount, and

changing a quantity by an arbitrarily small amount is a bit of an oxymoron. In our experiment, we observed transitions between states, so the adiabatic theorem is inapplicable. However, the Landau-Zener formula is too specific and limited to be applied to our situation, as we violate most of the assumptions that went into the model. There are certainly more than two accessible states in an atom. In deriving the formula, they assumed that the states only participate in one avoided crossing and deflect away from each other. We will find that pairs of states can have numerous avoided crossings with each other. The Landau-Zener formula is an asymptotic result, and it is unclear how applicable this is to an experiment where we have finite time scales, especially when keeping the fact that states have numerous avoided crossings in mind. The final nail in the coffin for the relevance of the Landau-Zener formula to our work is the fact that we observe interference patterns in our experiment. The Landau-Zener formula describes probabilities, not probability amplitudes, and does not maintain any phase information. The surefire way to keep the phase information and make sure that we get the right amplitudes after moving through an avoided crossing is to directly integrate the Schrodinger equation (cite forre). In the next chapter, we will discuss the techniques used to compute this time-evolution for Rydberg atom in the presence of a time-dependent electric field.

# Chapter 3

## Traversing the Stark Map

When an electric field is applied to an atom, this adds a perturbation to the Hamiltonian and shifts the energy levels. We can construct a plot of the energy spectrum against the electric fields strength to produce a diagram called a Stark map. In the first section of the chapter, we will discuss how to calculate the matrix elements of our Hamiltonian. Once we know the structure of the energy levels, we can use this to determine the time evolution of an arbitrary state. In our earlier work, we did not include the continuum states, so ionization had to be accounted for manually. At the end of the chapter, we will discuss the semi-classical methods used to obtain the ionization current and compare them with our experimental findings.

### 3.1 The Stark Effect

In order to construct a Stark map, we need to determine the matrix elements of our Hamiltonian. First, we will ignore the electric field term. In the absence of external fields, the states are described well by a hydrogen spectrum modified by quantum defects and fine structure. When one works with hydrogen and ignores fine structure, it is possible and convenient to work with the quantum numbers  $n$ ,  $l$ ,  $s$ ,  $m_l$ , and  $m_s$ , where  $n$  is the principal quantum number,  $l$  and  $s$  are the orbital and

spin angular momentum quantum numbers respectively ( $s = 1/2$  for an electron, we will omit this in some places), and  $m_l$  and  $m_s$  are the projections of these angular momentum onto the  $z$ -axis. However, when we include the fine structure, spin-orbit coupling necessitates working with the total angular momentum directly [5]. The total angular momentum operator  $\mathbf{J}$  is related to the orbital  $\mathbf{L}$  and spin  $\mathbf{S}$  angular momentum operators by the relation  $\mathbf{J} = \mathbf{L} + \mathbf{S}$ . This means that we need to work with new quantum numbers, namely, the total angular momentum  $j$ , which ranges from  $|l - s|$  when the orbital and spin angular momenta are oriented in opposite directions to  $l + s$  when they point in the same direction (so  $|l - s| \leq j \leq l + s$ ), and its projection  $m_j = m_l + m_s$  onto the  $z$ -axis. One can incorporate fine structure into the description of Rydberg states in the same way used for hydrogen. We will not deal with this here, as the details of this calculation are discussed in many textbooks on quantum mechanics [5]. It is worth mentioning that, as long as fine structure is ignored, the  $|n, l, s, m_l, m_s\rangle$  and  $|n, l, s, j, m_j\rangle$  bases both diagonalize the Hamiltonian. The initial Hamiltonian has eigenvalues

$$H_0 |n, l, j, m_j\rangle = -\frac{R_H}{(n - \delta_l)^2} |n, l, j, m_j\rangle,$$

where  $R_H$  is the Rydberg constant in energy units (13.6 eV) and  $\delta_l$  is the quantum defect due to the extended nature of the core [10]. One can expand the quantum defects in a series

$$\delta_l = \delta_{l,0} + \frac{\delta_{l,2}}{(n - \delta_{l,0})^2} + \frac{\delta_{l,4}}{(n - \delta_{l,0})^4} + \frac{\delta_{l,6}}{(n - \delta_{l,0})^6} \dots$$

and determine the coefficients from fitting experimental data. We used this expansion and the results from a number of experimental papers [11–13] in our calculation.

It follows that the matrix elements for the unperturbed electron-core interaction are

$$\langle n', l', j', m'_{j'} | H_0 | n, l, j, m_j \rangle = -\frac{R_H}{(n - \delta_l)^2} \delta_{n,n'} \delta_{l,l'} \delta_{j,j'} \delta_{m_j, m'_{j'}}. \quad (3.1)$$

Now, we will determine the matrix elements that arise from the electric field. We will take our field  $F$  to point along the  $z$ -axis. Up to an additive constant, this introduces a scalar potential  $-Fz = -Fr \cos \theta$ , which amounts to a potential energy term of the form  $V = eFr \cos \theta$ . When computing the matrix elements, it is convenient to do so in the decoupled basis. When working with coupled momenta, the coupled and decoupled bases are generally related via

$$|l, s, j, m_j\rangle = \sum_{m_l=-l}^l \sum_{m_s=-s}^s |l, s, m_l, m_s\rangle \langle l, s, m_l, m_s | l, s, j, m_j\rangle,$$

where the coefficients are referred to as Clebsch-Gordon coefficients [5]. Using the fact that  $s = 1/2$  in our case gives

$$|l, 1/2, j, m_j\rangle = \sum_{m_l=m_j \mp 1/2} |l, 1/2, m_l, m_j - m_l\rangle \langle l, 1/2, m_l, m_l - m_l | l, 1/2, j, m_j\rangle, \quad (3.2)$$

since we have  $m_j = m_l + m_s$ . We can write our matrix elements as

$$\begin{aligned} \langle n', l', j', m'_{j'} | V | n, l, j, m_j \rangle &= eF \sum_{m'=m'_{j'} \mp 1/2} \sum_{m=m_j \mp 1/2} \langle l', j', m'_{j'} | l', m', m'_{j'} - m' \rangle \\ &\times \langle l, m, m_j - m | l, j, m_j \rangle \langle n', l', m', m'_{j'} - m' | r \cos \theta | n, l, m, m_j - m \rangle. \end{aligned}$$

The radial and angular integrals are decoupled, so we may write

$$\begin{aligned} \langle n', l', j', m'_{j'} | V | n, l, j, m_j \rangle &= eF \sum_{m'=m'_{j'} \mp 1/2} \sum_{m=m_j \mp 1/2} \langle l', j', m'_{j'} | l', m', m'_{j'} - m' \rangle \\ &\times \langle l, m, m_j - m | l, j, m_j \rangle \langle l', m', m'_{j'} - m' | \cos \theta | l, m, m_j - m \rangle \langle n', l' | r | n, l \rangle. \end{aligned}$$

The angular term is directly computed in Arfken and Weber [14]

$$\begin{aligned} \langle l', m', m'_{j'} - m' | \cos \theta | l, m, m_j - m \rangle &= \delta_{m, m'} \delta_{m_j - m, m'_{j'} - m'} \\ &\times \left( \delta_{l', l+1} \sqrt{\frac{(l-m+1)(l+m+1)}{(2l+1)(2l+3)}} + \delta_{l', l-1} \sqrt{\frac{(l-m)(l+m)}{(2l-1)(2l+1)}} \right). \end{aligned}$$

Using this identity and the fact that  $\delta_{m, m'} \delta_{m_j - m, m'_{j'} - m'} = \delta_{m_j, m'_{j'}} \delta_{m_j - m, m'_{j'} - m'}$  finally gives

$$\begin{aligned} \langle n', l', j', m'_{j'} | V | n, l, j, m_j \rangle &= eF \delta_{m_j, m'_{j'}} \langle n', l' | r | n, l \rangle \\ &\times \sum_{m=m_j \mp 1/2} \langle l', j', m'_{j'} | l', m, m_j - m \rangle \langle l, m, m_j - m | l, j, m_j \rangle \\ &\times \left( \delta_{l', l+1} \sqrt{\frac{(l-m+1)(l+m+1)}{(2l+1)(2l+3)}} + \delta_{l', l-1} \sqrt{\frac{(l-m)(l+m)}{(2l-1)(2l+1)}} \right). \quad (3.3) \end{aligned}$$

The sum in Eq. 3.3 is straightforward to evaluate, the remaining work lies within computing the radial term

$$\langle n', l' | r | n, l \rangle = \int_0^\infty r^3 R_{n', l'}^*(r) R_{n, l}(r) dr.$$

We will determine the matrix elements by numerical integration. First, we must construct the solutions to the radial equation for a given set of quantum numbers.

Since the amplitude for a Rydberg state is localized far from the core, we can use hydrogenic solutions and maintain accuracy. It is useful to work in atomic units here to eliminate all units for computational purposes. In these units, the radial equation for hydrogen in a uniform electric field takes the form

$$\frac{d^2 R}{dr^2} + \frac{2}{r} \frac{dR}{dr} + 2(E + r^{-1})R - \frac{l(l+1)}{r^2}R = 0.$$

If we introduce the quantities  $x = \ln r$  and  $X = \sqrt{r}R$ , we find that

$$\frac{d^2 X}{dx^2} = g(x)X, \quad (3.4)$$

where  $g(x) = (l + 1/2)^2 + 2(E + e^{-x})e^{2x}$  [15]. The benefit of using Eq. 3.4 is that it is in the standard form for using the Numerov method. We discretize our variable as  $r_j = r_{\text{start}}e^{-jh}$ , where  $j$  is the step number and  $h$  is the step size. In this case, we are performing integration inward beginning at  $r_{\text{start}}$  and  $X$  is determined by the Numerov algorithm

$$X_{j+1} = \frac{X_{j-1}(g_{j-1} - 12/h^2) + X_j(10g_j + 24/h^2)}{12/h^2 - g_{j+1}}.$$

In these units, the classical turning point for an electron with energy  $-n^{-2}$  is at  $r = n^2$ . We expect the wave function to decay exponentially beyond this radius, so we begin our integration beyond this point, typical values are  $r_{\text{start}} \sim 2n^2$ . In order to determine  $X$ , we need to choose some initial conditions to start the algorithm. We used  $X_0 = 10^{-10}$  and  $X_1 = 10^{-5}$ , but the integration is fairly insensitive to these quantities. Once we have determined our two functions  $X$  and  $X'$  corresponding to

$n, l$  and  $n', l'$  respectively, we can calculate the matrix element

$$\langle n', l' | r | n, l \rangle = \frac{\sum_j X'_j X_j r_j^3}{\sqrt{(\sum_j X_j^2 r_j^2)(\sum_j X_j'^2 r_j^2)}}, \quad (3.5)$$

where we have used the fact that  $dr = -hr$  and the fact that the wave functions are real.

## 3.2 Stark Maps and Time Evolution

Now that we have determined the matrix elements of our Hamiltonian, we can calculate the spectrum and build Stark maps. In practice, we cannot diagonalize an infinite matrix with a computer, so we have to truncate it. If we make the matrix too large, we can't diagonalize it efficiently. We saw that the Stark effect couples different energy levels together. If the matrix is too small, we will ignore too many of these couplings and our spectrum will be inaccurate. We will return to address these concerns.

A sample Stark map is shown in Fig. 3.1. Note that both of the matrix elements in Eqs. 3.1 and 3.3 have a factor of  $\delta_{m_j, m'_j}$ . This means that different  $m_j$  values are decoupled from each other. One can also show that these matrix elements only depend on the absolute value  $|m_j|$ , so it makes sense to consider the subset of eigenvalues corresponding to a particular  $|m_j|$  value. In the Stark map shown here, we are looking at a subset of the spectrum for  $|m_j| = 1/2$  for  $^{85}\text{Rb}$ . Notice that the value of the allowed energies is clearly dependent on the value of the electric field and that the states participate in a large number of avoided crossings. The states that appear to diverge from a single point are called manifold states and have large angular momentum values, usually  $l \geq 3$ . The Stark map shows the  $n = 43$

and  $n = 44$  manifolds as well as the  $s, p, d$  states of larger  $n$  that lie between them. In practice, we find that including between 7 to 10 manifolds above and below the states of interest produces optimal results.

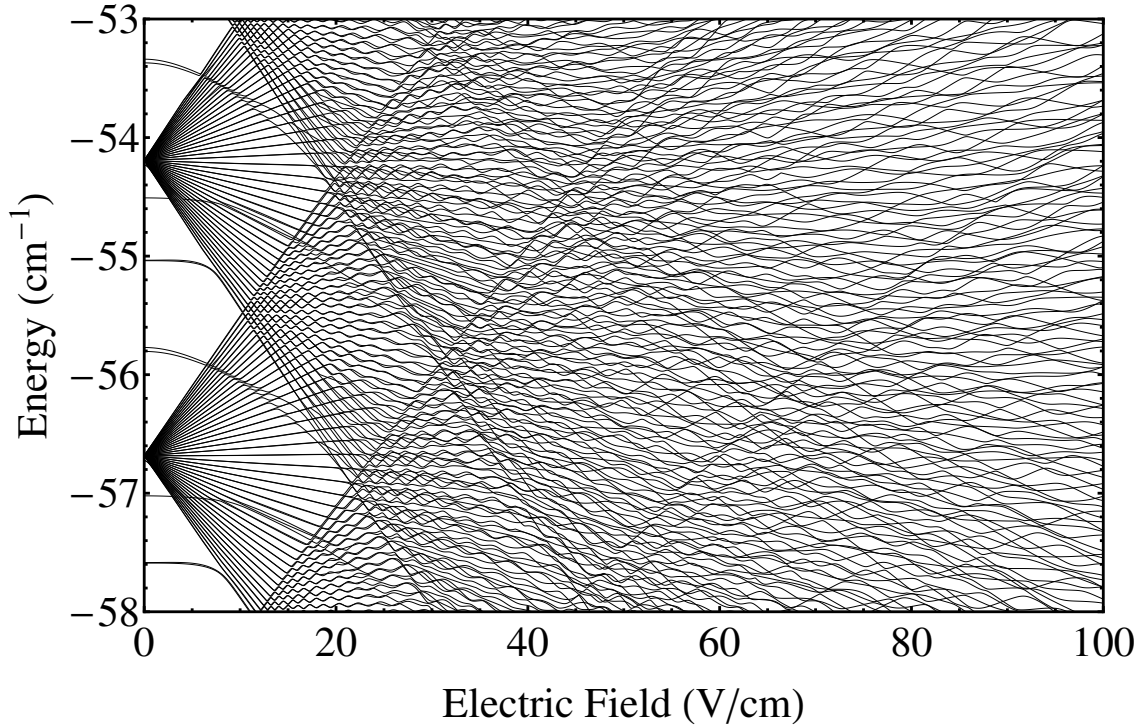


**Figure 3.1:** Stark map for the  $|m_j| = 1/2$  states of  $^{85}\text{Rb}$ . The  $n = 43, 44$  manifolds are shown with the  $s, p, d$  states of larger  $n$  that lie between them. Note that the energies depend on the electric field and that each state participates in a large number of avoided crossings.

Now we will concern ourselves with the time-dependence of the problem. In our experiment, the electric field is a linear function of time. Although this changing electric field induces a magnetic field, we find that magnetic effects are negligible, so we will neglect them. One can determine the time evolution of a state  $|\psi(t)\rangle$  by applying the time evolution operator [5]

$$|\psi(t_f)\rangle = U(t_i, t_f) |\psi(t_i)\rangle,$$

where the time evolution operator is related to the Hamiltonian by

$$U(t_i, t_f) = \exp\left(-\frac{i}{\hbar} \int_{t_i}^{t_f} H(t) dt\right).$$

In our model, we broke the time evolution up into small steps  $\Delta t$  and assumed that the Hamiltonian was nearly constant over this time step. We replaced the integral with a left-hand Riemann sum, giving

$$U(t_j, t_j + \Delta t) = \exp\left(-\frac{i}{\hbar} H(t_j) \Delta t\right).$$

Computing the exponential of a matrix is difficult when it is not diagonal, so we will cast the Hamiltonian into this form. Our matrix elements are constructed using hydrogen orbitals, that is, the eigenfunctions at zero electric field. We define  $\Lambda(t_j)$  to be the change of basis matrix that sends the zero field basis to the eigenbasis for the electric field at  $t_j$ . In this case, we can relate the constructed Hamiltonian  $H(t_j)$  to the diagonalized Hamiltonian  $H_D(t_j)$  by

$$H(t_j) = \Lambda^\dagger(t_j) H_D(t_j) \Lambda(t_j),$$

where the dagger indicates the adjoint, or conjugate transpose. This expression can be used to simplify the time evolution operator

$$U(t_j, t_j + \Delta t) = \Lambda^\dagger(t_j) \exp\left(-\frac{i}{\hbar} H_D(t_j) \Delta t\right) \Lambda(t_j). \quad (3.6)$$

This is much easier to calculate, as the exponential of a diagonal matrix is a diagonal matrix whose elements are the exponentials of the elements on the diagonal of the initial matrix. Given some initial state  $|\psi(0)\rangle$ , we can determine it at any time  $n\Delta t$

using the identity

$$|\psi(n\Delta t)\rangle = \left( \prod_{j=0}^{n-1} U(j\Delta t, (j+1)\Delta t) \right) |\psi(0)\rangle,$$

where this follows from the fact that  $U(t_3, t_2)U(t_2, t_1) = U(t_3, t_1)$ .

We applied this to our initial superposition of the  $|m_j\rangle$  states that formed from the Stark splitting of the  $37d_{5/2}$  level. A portion of the Stark map and the probability of finding the electron in a state at a given field are shown in Fig. 3.2. This Stark map superposes the maps for the different  $|m_j\rangle$  values. The probability of finding the electron in a state increases with the intensity of the color of the lines, and the  $|m_j| = 1/2$ ,  $|m_j| = 3/2$ , and the  $|m_j| = 5/2$  states correspond to red, blue, and green respectively. Notice that as the time and field increases, the probability is transferred to many other states, as the intensity of the colors decreases as you move to higher fields.

The black line in Fig. 3.2 is the classical ionization threshold. It is given by the formula

$$E = -6.12\sqrt{F},$$

where  $E$  is the energy in  $\text{cm}^{-1}$  and  $F$  is the electric field in  $\text{V/cm}$  [16]. A classical electron would be ionized if its energy was larger than the energy determined by the previous formula. It is a fairly good indicator of when ionization becomes important. This curve illustrates that all states are not ionized at the same time; higher energy states are ionized more readily than lower energy states. Therefore, we expect that our ionized current that arrives at the detector will be a distribution with some spread in time. Another important feature is that lines with different colors intersect the ionization threshold near the same field value. This means that

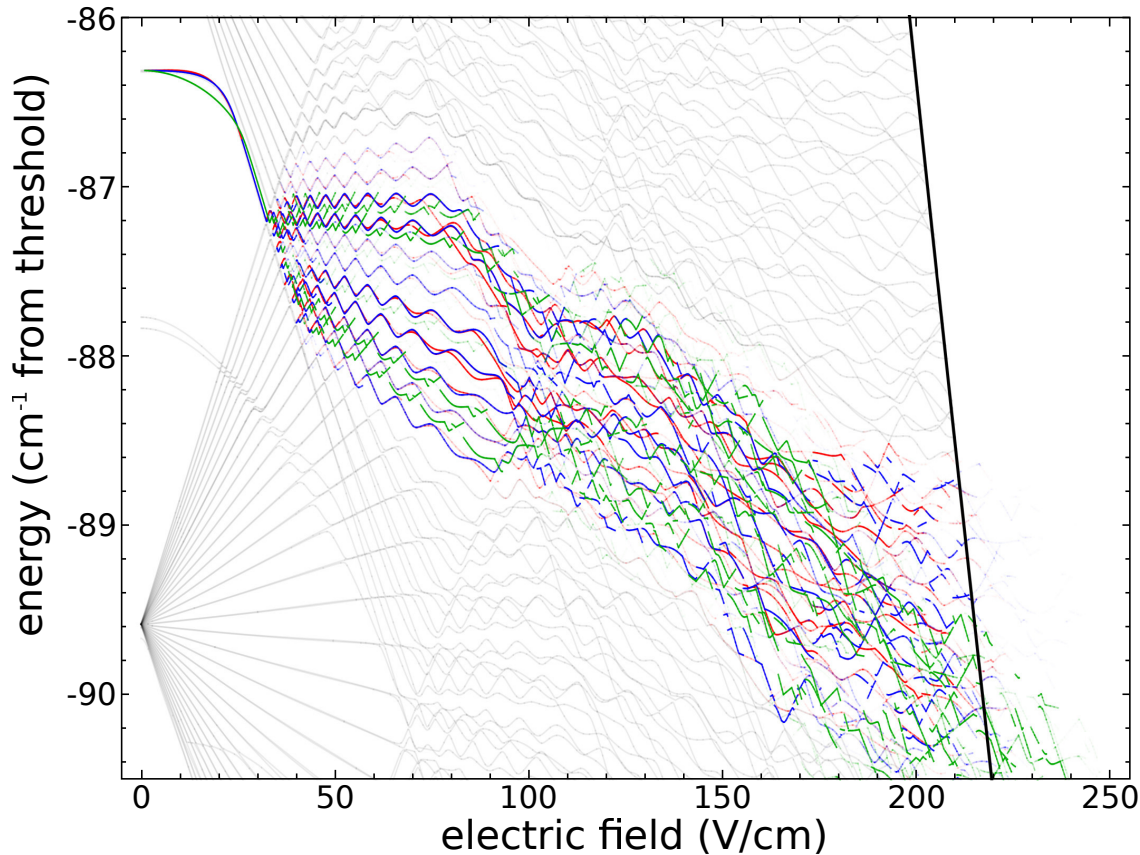


**Figure 3.2:** Portion of the Stark map where the initial state was a superposition of the different  $|m_j\rangle$  components of the  $37d_{5/2}$  state. Red, blue, and green correspond to  $|m_j| = 1/2, 3/2,$  and  $5/2$  respectively. The intensity of the color scales with the probability of finding the electron in that state. The black curve is the classical ionization threshold.

different  $|m_j\rangle$  components, with different phases, will ionize at the same time, so we expect to see some sort of interference at the detector.

### 3.3 The Semi-classical Ionization Current

In this section, we will discuss how we have extracted the ionization current from our quantum state near the ionization threshold. We use a semi-empirical formula

for the ionization rates derived by Damburg and Kolosov [17]

$$\Gamma = \frac{(4R)^{2n_2+m+1}}{n^3 n_2! (n_2 + m)!} \times \exp \left[ -\frac{2}{3}R - \frac{1}{4}n^3 F \left( 34n_2^2 + 34n_2 m + 46n_2 + 7m^2 + 23m + \frac{53}{3} \right) \right], \quad (3.7)$$

where  $R = (-2E_0)^{3/2}/F$ . In this expression,  $n$ ,  $n_1$ ,  $n_2$ , and  $m$  are the parabolic quantum numbers,  $E_0$  is the energy of the state, and  $F$  is the electric field. The energy of the state in parabolic coordinates was determined from fourth order perturbation theory. To express things in parabolic coordinates, we use Eq. 3.2 to move from the basis with coupled angular momenta to decoupled angular momenta. We can convert the decoupled basis to the parabolic basis by inverting the transformation given by Gallagher [10]

$$|n, n_1, n_2, m\rangle = \sum_l \langle n, l, m | n, n_1, n_2, m\rangle |n, l, m\rangle, \quad (3.8)$$

where the coefficient is

$$\langle n, l, m | n, n_1, n_2, m\rangle = (-1)^{1-n+m+n_1-n_2} \times \sqrt{2l+1} \begin{pmatrix} \frac{n-1}{2} & \frac{n-1}{2} & l \\ \frac{m+n_1-n_2}{2} & \frac{m-n_1+n_2}{2} & -m \end{pmatrix}. \quad (3.9)$$

The term with six elements in parentheses is the Wigner 3- $j$  symbol.

This ionization rate can be used to construct an ionization probability. The process of ionizing and the ionization rate is similar to the process of nuclear decay and decay rates. If we carry this reasoning to its conclusion, then the ionization rate is the inverse of the lifetime of the state. In this case, the probability of ionizing

per unit time goes as  $\exp(-\Gamma t)$ . If we begin at  $t = 0$ , normalization tells us that the probability of ionizing per unit time is

$$\dot{P}(t) = \Gamma \exp(-\Gamma t).$$

Now we will integrate this to find the probability of ionizing after some small time  $\Delta t$ . We can approximate this with a single left-hand Riemann sum to deduce that the ionization probability is  $\Gamma \Delta t$ . We multiplied each amplitude in parabolic coordinates by  $\sqrt{\Gamma \Delta t}$  and  $\sqrt{1 - \Gamma \Delta t}$  and stored the quantities separately. We computed the squared modulus of the first product and summed them over all of the parabolic coordinates to determine the ionization current at the given time. To make the current continuous, we multiplied each point by a gaussian distribution. We used the second product as the new amplitude, as we have subtracted off the part that has ionized. With this procedure, we cannot take the first products, add them, and then square them, as we could have destructive interference while the normalization of the state vector definitely decreases.

In Fig. 3.3, we have shown the experimental current (a) and the current produced by our model (b). The colored regions are unrelated to the different  $|m_j|$  values and indicate the regions that will be gated, or integrated over. There is a qualitative similarity between the current, but they are not identical, so we cannot use the same gates for the two spectra. We integrated each of the gates and plotted their area as a function of the delay time. The results for the experimental and theoretical currents are shown in Fig. 3.4 (a) and (b) respectively. Note that the red and blue lines are completely out of phase in (a), while this is not the case in (b). This suggests that we are not handling the phase correctly near ionization.

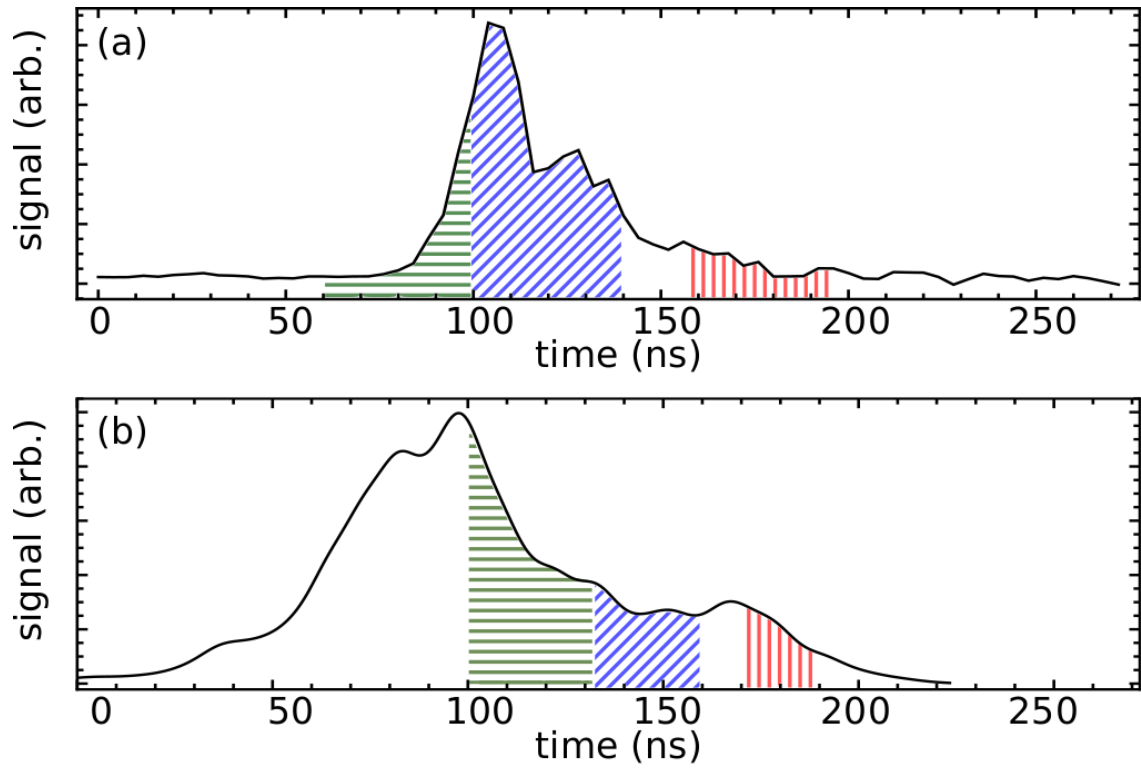


**Figure 3.3:** Experimental (a) and theoretical (b) ionization currents as functions of time. The colors here are unrelated to those in Fig. 3.2.

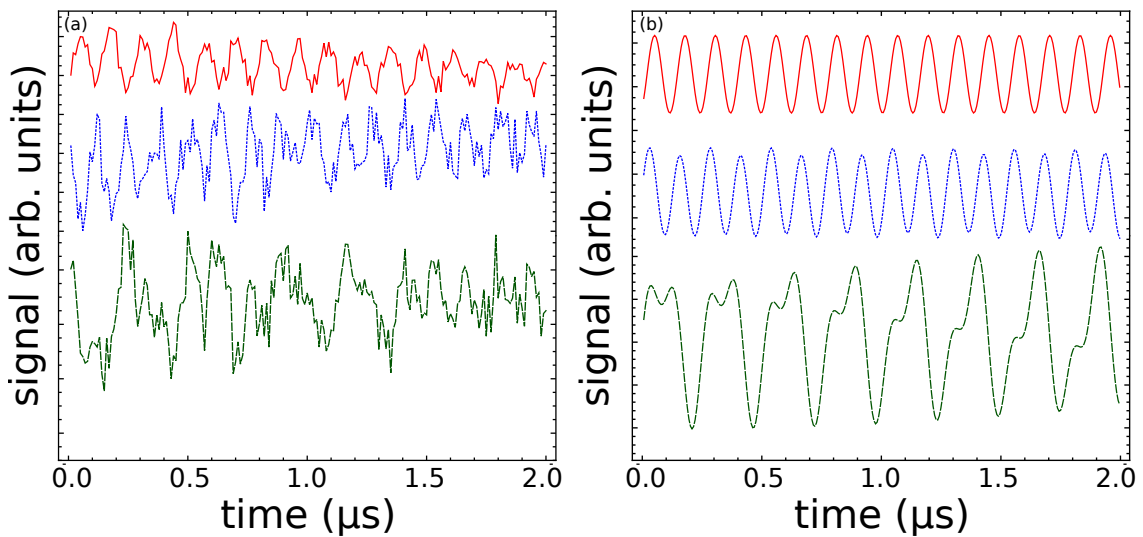


**Figure 3.4:** (a,b) Area under the regions in Fig. 3.3 (a,b) (respectively) as a function of the delay time. The color of the curves corresponds to the region that is integrated. In (a), the red and blue are completely out of phase, while this is not the case in (b).



# Chapter 4

## Including the Continuum States

In the previous chapter, we saw that we were getting the phase near ionization incorrect. There are a few problems with the approach that we have taken so far. First, our previous method of obtaining the ionization current is semi-classical and it is not clear if this approach deals with phase appropriately. A more serious problem is the fact that we are not including all of the relevant states and couplings to the system, so our phase near ionization is wrong because our energies near ionization are wrong.

In particular, we are ignoring the continuum, or free, states. These states have a continuous spectrum that goes from 0 to  $+\infty$ . To see that we should include these states, consider the relevant energies, shown in Fig. 4.1. The bound atomic states have some negative energy  $E$ , shown in red. The particle is always bound by the Coulomb potential energy  $V_C$ , shown in blue. Near the nucleus or core, we will have  $E > V_C$ . As we move away from the core, we find that  $E < V_C$ , even in the limit as we go to infinity, so the particle is permanently bound.

Applying an electric field introduces another potential energy term  $V_E$  that changes things. The sum of the potentials  $V_C + V_E$  is unbounded below as one moves to infinity in one direction. We can always find a region where  $E > V_C + V_E$  that extends out to infinity, so we see that an initially bound particle can always

tunnel through the potential barrier and escape to infinity. This process is known as tunnel ionization, and it is the mechanism responsible for ionizing our atoms. We see that, in the presence of a uniform electric field, there are no permanently bound atomic states. Since our wave functions need to be able to escape to infinity and this possibility is not captured by using bound states at zero field, we need to include the coupling to the free states.

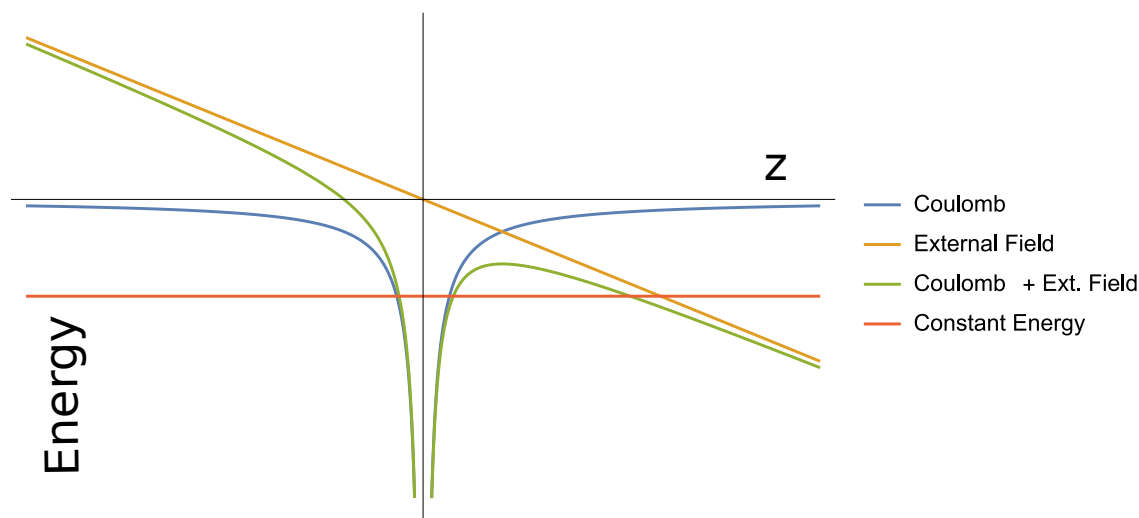


**Figure 4.1:** Potentials for an attractive Coulomb interaction and a uniform electric field with  $x = y = 0$ . Since the sum of the potentials is unbounded below as one goes to infinity, there are no permanently bound states.

## 4.1 Hypergeometric Functions

In this section, we will discuss the essential results from the theory of hypergeometric functions. The hydrogenic continuum states are easily expressed in terms of these functions. Additionally, there is a closed form for the integrals that occur when describing the coupling of continuum and bound states that is also expressed in terms of these functions. The hypergeometric functions converge slowly, and having

this closed form avoids many errors that may be introduced by approximating the function and integrating numerically out to infinity.

Before defining the hypergeometric functions, it is convenient to introduce the *Pochhammer symbols*  $(\alpha)_k$  for any complex  $\alpha$  and positive integer  $k$ . These are defined as

$$\begin{aligned} (\alpha)_k &= (\alpha)(\alpha + 1)\dots(\alpha + (k - 1)) \\ &= \prod_{j=0}^{k-1} (\alpha + j). \end{aligned} \quad (4.1)$$

The second formulation provides a natural setting to generalize the symbols to include the case  $k = 0$ . A product is said to be empty whenever the lower index is larger than the upper index. The empty product is defined to be 1, so it is natural to take  $(\alpha)_0 = 1$ . It is clear that the symbols satisfy the identity

$$(\alpha)_{k+1} = (\alpha)_k(\alpha + k). \quad (4.2)$$

Suppose we have two finite collections of complex numbers of size  $p$  and  $q$ , say  $\{a_1, \dots, a_p\}$  and  $\{b_1, \dots, b_q\}$  respectively. The *generalized hypergeometric function*  ${}_pF_q$  is defined as

$${}_pF_q(a_1, \dots, a_p; b_1, \dots, b_q; z) = \sum_{n=0}^{\infty} \frac{\prod_{j=1}^p (a_j)_n}{n! \prod_{k=1}^q (b_k)_n} z^n, \quad (4.3)$$

where  $z$  is any complex number. Under complex conjugation, note that the hypergeometric function satisfies the identity

$${}_pF_q(a_1, \dots, a_p; b_1, \dots, b_q; z)^* = {}_pF_q(a_1^*, \dots, a_p^*; b_1^*, \dots, b_q^*; z^*).$$

There are two particular cases that will be of interest to us. The first is the *confluent hypergeometric function* in the case that  $p = q = 1$ , and the second is the *ordinary hypergeometric function* in the case that  $p = 2$  and  $q = 1$ .

### 4.1.1 The Confluent Hypergeometric Equation

The confluent hypergeometric functions have a close connection with the *confluent hypergeometric equation*:

$$x \frac{d^2 u}{dx^2} + (c - x) \frac{du}{dx} - au = 0. \quad (4.4)$$

This is a second-order, linear, ordinary differential equation, so, for fixed  $a$  and  $c$ , the solution space is two dimensional. As the name suggests, the two linearly independent solutions are easily expressed in terms of the confluent hypergeometric functions. As a first attempt at a solution, we posit a series solution:

$$u(x) = \sum_{n=0}^{\infty} a_n x^{n+s},$$

for some fixed number  $s$ . Substituting the series into the differential equation and demanding consistency implies that  $s = 0$  or  $s = 1 - c$ . One can use this to show that the most general solution is

$$u(x) = A {}_1F_1(a; c; x) + B x^{1-c} {}_1F_1(1 + a - c; 2 - c; x), \quad (4.5)$$

where  $A$  and  $B$  are arbitrary constants. It turns out that the radial equation that describes the energy spectrum of a hydrogen-like atom can be cast into the form of Eq. 4.4. Once we reduce the radial equation to this form, we can immediately

determine the eigenfunctions since it has been reduced to a solved problem.

## 4.2 Hydrogenic Continuum States

In this section, we will derive the form of continuum states and discuss how to incorporate the bound-continuum and continuum-continuum coupling into the existing framework. We will assume that the continuum states correspond to the continuum states for rubidium. Besides having an exact result for rubidium, this seems to be the closest approximation. We do not expect the interaction of the bound electrons to alter the continuum states much, as the continuum states are not square integrable and are more likely to be found far away from the nucleus. This is also a better model than using some other states, say those for the harmonic oscillator, instead.

We will begin by mimicking a standard derivation for the bound eigenfunctions of hydrogen as found in a standard quantum mechanics textbook [5]. The derivations have most of the steps in common, but some of the arguments have to be modified, as the continuum states are not square integrable. The radial equation for hydrogen is

$$\frac{d}{dr} \left( r^2 \frac{dR}{dr} \right) - \frac{2m}{\hbar} \left( -\frac{e^2}{4\pi\epsilon_0 r} + \frac{\hbar^2 l(l+1)}{2mr^2} - E \right) R = 0. \quad (4.6)$$

If we choose to work with  $E > 0$ , we can define the following unitless coordinates

$$\lambda = \frac{e^2}{4\pi\epsilon_0 \hbar} \sqrt{\frac{m}{-2E}} \quad \rho = \frac{r}{\hbar} \sqrt{-8mE},$$

and use this to re-express the hydrogen Hamiltonian in Eq. 4.6 in the form

$$\frac{d^2 R}{d\rho^2} + \frac{2}{\rho} \frac{dR}{d\rho} + \left( \frac{\lambda}{\rho} - \frac{l(l+1)}{\rho^2} - \frac{1}{4} \right) R = 0. \quad (4.7)$$

Note that our unitless coordinates are undefined when  $E = 0$ . There are some subtleties involved here, but they are not relevant for our purposes. We will address this point later, but it is not a relevant problem.

Now we will study the limiting behavior of the solutions to this differential equation. First, we will study the behavior  $\rho$  becomes arbitrarily small. In this case, we keep the derivatives and the term with the largest power of  $\rho$  in the denominator, so Eq. 4.7 approximately becomes

$$\frac{d^2 R}{d\rho^2} + \frac{2}{\rho} \frac{dR}{d\rho} - \frac{l(l+1)}{\rho^2} R = 0.$$

There are two solutions to this differential equation:  $\rho^l$  and  $\rho^{-(l+1)}$ . We now argue that this second solution should be rejected. First, we deal with the case of  $l > 0$ . The modulus of the radial part of the wave function goes as  $r^{-2l-2}$  near the origin. Since the volume element is  $r^2 dr$ , our radial integrand is at least  $r^{-2}$ . We expect a finite probability of finding the electron in a closed and bounded region of space (think of locating a particle in a plane wave state inside of a cube). This is not integrable in the limit as  $r \rightarrow 0$ , so we must reject this solution. Now we deal with the case where  $l = 0$ . In this case, the limiting differential equation for  $r$  is

$$0 = \frac{d^2 r^{-1}}{dr^2} + \frac{2}{r} \frac{dr^{-1}}{dr} = \nabla^2 r^{-1}.$$

However, it is well-known that the Laplacian of  $1/r$  is proportional to a Dirac delta

function, which is not zero [18]. Therefore, the limiting behavior as  $\rho$  tends to zero must be  $\rho^l$ .

In the bound state case, we know that the wave functions vanish at infinity, and this gives another constraint. However, we cannot impose an analogous boundary condition on the continuum states. Nonetheless, it is still convenient to factor the radial wave function for the continuum states in the same way as the bound states. Without loss of generality, we can write

$$R(\rho) = \rho^l e^{-\rho/2} w(\rho),$$

where  $w$  is some undetermined function whose lowest order of  $\rho$  is a non-zero constant; one may regard this as defining  $w$ . When working with bound states, the exponential in this factoring was decaying, but in this case, it is oscillating. Substituting this factorization into Eq. 4.7 gives the differential equation

$$\rho \frac{d^2 w}{d\rho^2} + (2l + 2 - \rho) \frac{dw}{d\rho} - (1 + l - \lambda)w = 0.$$

Looking back at Eq. 4.4, we see that this has precisely the same form as the confluent hypergeometric equation! We make the identifications  $a = 1 + l - \lambda$  and  $c = 2l + 2$ . Looking back at the most general solution in Eq. 4.5, the coefficient for the second solution must be zero, as this term has additional powers of  $\rho$  that do not obey the required small  $\rho$  behavior. It follows that the solutions can be expressed as

$$R(\rho) = A \rho^l e^{-\rho/2} {}_1F_1(1 + l - \lambda, 2l + 2, \rho),$$

for some constant  $A$ . Note that these modified arguments apply to the bound states as well, as we have not explicitly used the fact that  $E > 0$ . If we choose to study the

bound states, we get another boundary condition at infinity. When this condition is imposed, we find that the confluent hypergeometric function coincides with the associated Laguerre polynomials. Turning our attention to the continuum states with  $E > 0$ , we can determine  $A$  by requiring that the continuum eigenfunctions are delta-normalized, that is,

$$\int \psi_{E'}^*(\vec{r})\psi_E(\vec{r})dV = \delta(E - E').$$

This calculation was performed by Ugray and Shiell [19], and they determined that the radial component of the delta-normalized continuum eigenfunctions was

$$R_{E,l}(r) = \sqrt{\frac{2 \prod_{s=0}^l (1 + Es^2/R_H)}{(1 - \exp(-\pi\sqrt{4R_H/E}))R_H a_0^3 (2l+1)!}} (2r/a_0)^l \exp\left(\frac{ir}{a_0}\sqrt{\frac{E}{R_H}}\right) \times {}_1F_1\left(l+1 - i\sqrt{\frac{R_H}{E}}, 2l+2, -2i\frac{ir}{a_0}\sqrt{\frac{E}{R_H}}\right), \quad (4.8)$$

where  $a_0$  is the Bohr radius and  $R_H$  is the Rydberg constant in energy units.

### 4.3 Coupling to the Continuum

Now that we have determined the continuum eigenfunctions, the next task is to calculate their coupling to the bound states and other continuum states. It is clear that we need bound-continuum coupling in order for ionization process to occur without artificially subtracting a rate. One can view the addition of the continuum states as adding some positive energy levels to the Stark map. Their coupling to the bound states will drive them towards the bound states. If we neglect continuum-continuum coupling, the continuum states will only have one avoided crossing with

the bound states, deflect towards positive energy, and never return. There are two problems with this. Since an electron ionizes when it transitions to a continuum state, we need to keep the continuum near the bound states to ensure that we have the proper coupling and amplitude transferred to the continuum. The energies of our bound states are incorrect near the ionization threshold, and they will only receive a small correction if they interact with the continuum once. In order to ensure that we get these energies and the phase correct, we need to keep the continuum near the bound states.

The matrix elements depend on the computation of the radial term. Since the solutions are products of confluent hypergeometric functions, powers of the radius, and exponential functions, it suffices to determine integrals of the form

$$J_c^{s,p}(a, a') = \int_0^\infty e^{-hr} r^{c-1+s} {}_1F_1(a; c; kr) {}_1F_1(a'; c-p; k'r) dr. \quad (4.9)$$

Karule [20] determined this integral in the case where  $s$  and  $p$  are positive integers and  $\Re(h) > 0$ . This relations hold when one of the states is a bound state. She found that the integrals could be expressed in closed form

$$J_c^{s,p}(a, a') = \Gamma(c+s) h^{-c-s} (1 - k'/h)^{-a'} (1 - k/h)^{-a} \sum_{m=0}^{s+p} \left[ \frac{(a')_m (-s-p)_m (k')^m}{(c-p)_m (k'-h)^m m!} \right. \\ \left. \times \sum_{r=0}^{s+m} \frac{(a)_r (-s-m)_r k^r}{(c)_r (k-h)^r r!} {}_2F_1 \left( a+r, a'+m; c+r; \frac{-4kk'}{(k'-k)^2} \right) \right]. \quad (4.10)$$

This can be used to determine the bound-continuum coupling, but the assumptions that went into deriving this fail for continuum-continuum coupling.



# Chapter 5

## Future Work

First, I need to do some further work to turn this project into a computationally feasible task. There is a method proposed by Cowan [21] that discusses modeling the continuum by discrete chunks. This involves integrating the continuum states and the matrix elements over some width in the energy spectrum  $\Delta E$ . The effect of this will be to add new bands to the Stark map.

The implementation discussed only describes bound-continuum coupling. The next step forward is to include continuum-continuum coupling for the reasons that I have discussed. The straightforward calculation of these quantities is challenging, as one can make simple arguments to show that this coupling is divergent. If this is the case, then I will try to perform the integration procedure, as I expect this to smooth out the divergences. Once I have determined how to include the continuum-continuum coupling and model the continuum as discrete states, the final step will be to test the implementation and determine the optimal number of orbital angular momentum states that need to be included, as well as the total width and resolution  $\Delta E$  of the continuum states.



# Bibliography

- [1] R. C. Stoneman, D. S. Thomson, and T. F. Gallagher. Microwave multi-photon transitions between Rydberg states of potassium. *Physical Review A*, 37(5):1527–1540, March 1988.
- [2] Xinsheng Tan, Dan-Wei Zhang, Zhentao Zhang, Yang Yu, Siyuan Han, and Shi-Liang Zhu. Demonstration of Geometric Landau-Zener Interferometry in a Superconducting Qubit. *Physical Review Letters*, 112(2):027001, January 2014.
- [3] Y. P. Zhong, Z. L. Wang, J. M. Martinis, A. N. Cleland, A. N. Korotkov, and H. Wang. Reducing the impact of intrinsic dissipation in a superconducting circuit by quantum error detection. *Nature Communications*, 5:3135, January 2014.
- [4] Rachel Feynman, Jacob Hollingsworth, Michael Vennettilli, Tamas Budner, Ryan Zmiewski, Donald P. Fahey, Thomas J. Carroll, and Michael W. Noel. Quantum interference in the field ionization of Rydberg atoms. *Physical Review A*, 92(4):043412, October 2015.
- [5] Mark Beck. *Quantum Mechanics: Theory and Experiment*. Oxford University Press, New York, 1st edition, May 2012.
- [6] Stephen H. Friedberg, Arnold J. Insell, and Lawrence E. Spence. *Linear Algebra*. Pearson, Upper Saddle River, N.J, 4th edition, November 2002.

- [7] David C. Lay. *Linear Algebra and Its Applications*. Pearson, Boston, 4th edition, January 2011.
- [8] Leslie E. Ballentine. *Quantum Mechanics: A Modern Development*. World Scientific, 1998.
- [9] Jan R. Rubbmark, Michael M. Kash, Michael G. Littman, and Daniel Kleppner. Dynamical effects at avoided level crossings: A study of the Landau-Zener effect using Rydberg atoms. *Physical Review A*, 23(6):3107–3117, June 1981.
- [10] Thomas F. Gallagher. *Rydberg Atoms*. Cambridge University Press, Cambridge, New York, 1st edition, November 2005.
- [11] K. Afrousheh, P. Bohlouli-Zanjani, J. A. Petrus, and J. D. D. Martin. Determination of the  $^{85}\text{Rb}$ -series quantum defect by electric-field-induced resonant energy transfer between cold Rydberg atoms. *Physical Review A*, 74(6):062712, December 2006.
- [12] M. F. F. and J. P. Hansen. Selective-field-ionization dynamics of a lithium  $m=2$  Rydberg state: Landau-Zener model versus quantal approach. *Physical Review A*, 67(5):053402, May 2003.
- [13] Jianing Han, Yasir Jamil, D. V. L. Norum, Paul J. Tanner, and T. F. Gallagher.  $\text{Rb}$  quantum defects from millimeter-wave spectroscopy of cold  $^{85}\text{Rb}$  Rydberg atoms. *Physical Review A*, 74(5):054502, November 2006.
- [14] George B. Arfken, Hans J. Weber, and Frank E. Harris. *Mathematical Methods for Physicists, Seventh Edition: A Comprehensive Guide*. Academic Press, Amsterdam ; Boston, 7 edition edition, January 2012.

- [15] Myron L. Zimmerman, Michael G. Littman, Michael M. Kash, and Daniel Kleppner. Stark structure of the Rydberg states of alkali-metal atoms. *Physical Review A*, 20(6):2251–2275, December 1979.
- [16] F. Robicheaux, C. Wesdorp, and L. D. Noordam. Selective field ionization in Li and Rb: Theory and experiment. *Physical Review A*, 62(4):043404, September 2000.
- [17] R. J. Damburg and V. V. Kolosov. A hydrogen atom in a uniform electric field. III. *Journal of Physics B: Atomic and Molecular Physics*, 12(16):2637, 1979.
- [18] Paul Adrien Maurice Dirac. *The Principles of Quantum Mechanics*. Clarendon Press, January 1981.
- [19] Lisa Madeleine Ugray and Ralph C. Shnell. Elucidating Fermi’s Golden Rule via bound-to-bound transitions in a confined hydrogen atom. *arXiv:1206.2905 [physics]*, June 2012. arXiv: 1206.2905.
- [20] E. Karule. Integrals of two confluent hypergeometric functions. *Journal of Physics A: Mathematical and General*, 23(11):1969, 1990.
- [21] Robert D. Cowan. *The Theory of Atomic Structure and Spectra*. University of California Press, Berkeley, September 1981.
- [22] James B. Seaborn. *Hypergeometric Functions and Their Applications*. Springer, New York, softcover reprint of the original 1991 1st edition, September 2011.
- [23] Hans A. Bethe and Edwin E. Salpeter. *Quantum Mechanics of One- And Two-Electron Atoms*. Martino Fine Books, Mineola (NY), 2014 reprint of 1957 edition, April 2014.

- [24] Clarence Zener. Non-Adiabatic Crossing of Energy Levels. *Proceedings of the Royal Society of London A: Mathematical, Physical and Engineering Sciences*, 137(833):696–702, September 1932.
- [25] Ryan Murray. Tunnel Ionization in Strong Fields in atoms and molecules and its applications.
- [26] Immanuel Bloch. Ultracold quantum gases in optical lattices. *Nature Physics*, 1(1):23–30, October 2005.
- [27] Nasser Saad and Richard L. Hall. Integrals containing confluent hypergeometric functions with applications to perturbed singular potentials. *Journal of Physics A: Mathematical and General*, 36(28):7771, 2003.
- [28] Wenhui Li, I. Mourachko, M. W. Noel, and T. F. Gallagher. Millimeter-wave spectroscopy of cold Rb Rydberg atoms in a magneto-optical trap: Quantum defects of the  $n_s$ ,  $n_p$ , and  $n_d$  series. *Physical Review A*, 67(5):052502, May 2003.
- [29] John S. Townsend. *A Modern Approach to Quantum Mechanics*. Univ Science Books, Sausalito, Calif, 2 edition, February 2012.
- [30] John S. Townsend. *Quantum Physics: A Fundamental Approach to Modern Physics*. University Science Books, 2010.